EUROPEAN ORGANIZATION FOR NUCLEAR RESEARCH

CERN/EP 80-93
9 June 1980

SEARCH FOR NARROW BARYONS IN THE $\pi^- p$ TOTAL CROSS SECTION BETWEEN 2 AND 14 GeV/c

CERN[1], Collège de France[2], Ecole Polytechnique[3] Collaboration

E. Barrelet[3], P. Baillon[1], M. Benayoun[2], J. Chauveau[1], D. Chew[3*], M. Ferro-Luzzi[1], J. Kahane[2], D. Lellouch[3], P. Leruste[2], P. Liaud[3], F. Moreau[3], J.M. Perreau[1], J. Séguinot[1**], R. Sené[2], J. Tocqueville[2] and M. Urban[3]

ABSTRACT

A high-statistics search for resonances in the $\pi^- p$ total cross section has been carried out over the incident momentum region from 2 to 14 GeV/c. The measurements were performed with a transmission technique using multiwire proportional chambers in place of the conventional counter arrays. A microprocessor unit was used for the on-line analysis of the data, allowing a total of $\sim$ 50 000 events to be examined in a 300 ms burst. The search aimed at detecting the possible formation in $\pi^- p$ collisions of narrow non-strange baryon resonances. The momentum region was uniformly scanned with a total of $\sim$ 4500 measurements in fixed fractional momentum steps of $dP/P = 5\ 10^{-4}$. The relative statistical precision of each measurement was $d\sigma/\sigma = \pm 0.3\%$. Within these limits no significant structure was detected.

Submitted to Physics Letters B

(*) Permanent address, LBL, University of California, USA.

(**) Supported by CNRS and Université de Caen, France.

0009P/MFL/ed

1. INTRODUCTION

The motivation for this study is the same as that of the companion experiment of ref. [1], i.e. the hope of finding narrow structures in the $\pi^- p$ cross section pointing to the formation of non-strange baryon resonances. The difference with respect to the approach of ref. [1] is that here the evidence for structures has been looked for in the total $\pi^- p$ cross section instead of the large-angle elastic scattering. One advantage is that the resonant signal is now expected to be proportional to the elasticity x instead of x^2 thus improving the chances to see resonances with smaller elasticity than in the elastic channel. Another appealing feature is of having access to a very high statistical precision; the total cross section in the region of the experiment (2 to 14 GeV/c) is of the order of 30 mb, to be compared with the few nanobarns examined in ref. [1]. Unfortunately, at high energy this apparent advantage is counterbalanced by problems of its own. The background under the hypothetical resonance is now several orders of magnitude larger than in ref. [1] and one is confronted with possible non-statistical fluctuations which must be well understood and kept under tight control if the tiny signal expected from the resonance is to be unambiguously identified. We believe that we have achieved the above requirement.

The measurements have been done in the conventional "transmission" approach with three notable differences. First, we used proportional wire chambers instead of the usual concentric set of circular counters of diminishing diameter. Secondly, we analysed the incident momentum with a resolution $dP/P \sim 5\ 10^{-4}$. The first allows a much better control over the measurements than the one provided by the usual set of large and thick counter arrays, the second permits the narrow structure search which was the purpose of the experiment. Finally, the analysis was performed completely on-line with the data taking; this feature was essential because it gave us access to a complex series of reproducibility tests which otherwise would have been too awkward and prohibitively time-consuming to be performed.

2. MEASUREMENTS

The experiment has been performed at the CERN Proton Synchrotron on the P_{17} beam in the East Hall. Most of the apparatus was the same that was used for the measurement of the large-angle differential cross section. We refer to the description of the latter [1] for the details of the equipment. All but the actual data taking was conducted in parallel with the above experiment. In particular, the focusing spectrometer with its chambers, the target and the veto box were the same. The difference in apparatus was essentially downstream of the target. Fig. 1 shows the set-up with the part of the equipment used specifically by this experiment; the complete set-up of ref. [1], although not drawn, was in place.

From the section of the incident branch preceding the BM magnets only the x plane of W_1 was used. A total of five coordinates (three x's and two y's) was employed for the incident track reconstruction. The trigger logic was very simple, being provided by the H_2 hodoscope alone. An artificial deadtime amounting to 250 ns before and 70 ns after the accepted trigger was introduced as a precaution against accidentals in the chambers.

Downstream of the target were two multiwire proportional chambers close together, WF_1 and WF_2(*). The first gave x and y information over a region of 19 x 19 cm^2 with a coordinate spacing of 1 mm; the second gave x and y over 26 x 26 cm^2 with a coordinate spacing of 2 mm. One metre beyond these chambers was an iron screen 80 x 80 cm^2 in cross section, followed by two scintillator counters (ST_1 and ST_2) covering the above surface and providing the muon signal (S_μ).

The liquid hydrogen target (6 cm in diameter, 25 cm in length) had been the object of special precautions as regards its temperature stabilization. Upper and lower jackets with circulating liquid hydrogen were in contact with the target proper, insuring a high degree of insulation and a guarantee against boiling. The resulting temperature stability, hence the maximum density variation, was of 1 part over $\sim$ 10 000. This temperature was continuously monitored during data taking.

(*) When scanning the 2 to 5 GeV/c momentum region these chambers were at a distance of 120 cm from the target centre; from 5 to 14 GeV/c the distance was increased to 380 cm.

The on-line analysis provided a reconstruction, event-by-event, of the incident particle trajectory and that of the secondary track whenever one and only one passed through the downstream chambers. Depending on the observed coordinate configuration and on the status of the VB and S_μ signals the result of the calculation was entered into one or another of several momentum and angle histograms. These histograms represent the result of the measurement for each momentum setting and were stored on tape.

The on-line calculations were carried out in an average of 5 μs per event via a programmable microprocessor unit (arithmetic and logic unit AMD2900 with 168 ns basic cycle, 1024 16-bit words of instructions, 2048 words of data) backed by an HP-2100 computer through standard Camac controllers.

The interaction rate at our energies being of the order of 2 to 3%, a sampling procedure was introduced in order to apportion the time optimally between the analysis of particles which go through the target without interacting and the analysis of those which interact. One particle out of eleven was systematically followed through the program chain; this was sufficient for the collection of an adequate statistics on the incident momentum spectrum. In the other ten cases each event was first examined for signs of interaction, dropping it without further analysis if some simple non-interaction criteria were satisfied. The above operation, using the secondary chambers, needed only a small fraction of the total microprocessor chain and resulted in a purified sample of interacting events. These were then passed on to the rest of the chain for full analysis.

The complete microprocessor operation followed the three-step course briefly outlined below. In the first stage ($\sim$ 3.6 μs) the beam chambers were inspected to see if the minimum required number of coordinates was available. If not, the event was dropped. Otherwise (and only in the case of non "beam-sample" events) the downstream chamber WF_1 was examined in order to find out if both the x- and the y-coordinates were inside the multiple scattering shadow of the beam. Some 88% of the non-interacting particles was detected at this stage and processed no further. The second stage ($\sim$ 10 μs) dealt with the beam cuts and the incident momentum calculation. Any occurrence of multiple hits in the beam chambers

condemned the event. When one and only one coordinate was present per beam chamber plane, the momentum difference dP with respect to the nominal setting was calculated as follows:

$$dP = a_o + a_1 x_1 + a_2 x_2 + a_3 x_3 .$$

The expansion coefficients, a_i, were determined prior to the experiment with a Monte-Carlo simulation. A cut was applied on the value obtained for dP as well as on the track intersect with the W_2 and W_3 chambers. This was done in order to satisfy the phase-space boundary criteria

$$dx = x_3 - b_1 x_2 - b_2 ,$$

$$dy = y_3 - c_1 y_2 - c_2 ,$$

where the coefficients b_i and c_i are functions of dP. These coefficients were predetermined, at each setting, on the basis of short calibration runs. As a result of the second stage calculations, 10 out of 12 non-interacting particles undetected in the first stage were rejected. The remaining particles had their momentum and direction unambiguously determined. The third stage ($\sim$ 40 μs) dealt with the interaction products. Here the events were distributed among various categories depending on the coordinate configuration in the secondary chambers. The following three main categories occurred. The first (representing on the average $\sim$ 25% of the total) corresponded to non-interacting beam tracks associated to multiple hits in the secondary chambers and for this reason misinterpreted by the simplified calculations of the first-stage filter. The second ($\sim$ 15% of the total) corresponded to events which could not be assigned an unambiguous interpretation. These events, too complex for the microprocessor to deal with, were labelled according to their general characteristics, counted and later used as corrections on the measured cross sections. Special runs were made in order to understand the origin of these events. It was found that about half of them are due to the forward emission of more than one charged track; these were then considered to be genuine interactions. The other half were simple one-track events associated to chamber inefficiency and/or overefficiency (accidentals, δ rays, etc.). The third category ($\sim$ 60% of the total) consisted of the unambiguously interpretable events. Here the interaction resulted in either a single track in the secondary chambers or in interaction products

missing altogether these chambers. These events were used to calculate the total cross section. Their measured incident momentum was entered in one or other of two "momentum spectrum" histograms (M_1 and M_2) depending on the secondary track being detected or missed by the chambers. The scattering angle, when available, was also entered (independently of momentum) in two "angular distribution" histograms, one for the small-angle region ($|t| \leq 10^{-2}$ GeV^2), the other for the large-angle region from $|t| > 10^{-2}$ GeV^2 up to $|\theta| \leq 30$ mrad. Various other histograms were also recorded, such as the momentum spectrum of the unscattered particles (the "normalization" spectrum), the angular distribution and momentum spectrum of the tracks associated with an S_μ signal (the "muon" spectrum), of those associated with a VB signal (the "inelastic" spectrum), etc.

A total of 57 momentum settings was taken. Each setting covered a total momentum bite of $\sim 4\%$; the spacing between settings was 3.5%. The typical trigger rate during the experiment was $\sim$ 50 000 incident particles for PS burst of 300 ms; these triggers resulted in some 3000 beam-sample events and $\sim$ 1000 interaction events. Full- and empty-target runs were taken at each setting, with an accumulation of $\sim 2.5\ 10^8$ and $\sim 0.8\ 10^8$ events respectively. These numbers were reached over a total of $\sim$ 15 h per setting. The statistical precision obtained was $\pm$ 0.3% on the total cross section for each dP/P bin of $\pm\ 2.5\ 10^{-4}$. The total number of incident pions used in the whole experiment was $\sim 2\ 10^{10}$.

3. ANALYSIS

An example of the basic data as they emerge from the microprocessor at each momentum setting is shown in figs 2(a) to 2(f). The histograms in the left-hand column refer to the full-target runs at 4.11 GeV/c, those in the right-hand column to the empty-target runs at the same setting. Histograms (a) and (b) are the momentum spectra (in 80 dP/P bins of $5 \cdot 10^{-4}$) for the events in which one and only one track was unambiguously identified by the secondary chambers (M_1 of the above description). Histograms (c) and (d) are those for the events where no track at all was found in the secondary chambers (M_2 of the above description). Histograms (e) and (f) are the momentum spectra of the beam particles, independently of what happened in the target (i.e. the "beam sample" histograms). The lowest two

histograms, (g) and (h), are respectively the sum of (a) and (c) divided by (e) and the sum of (b) and (d) divided by (f). Hence they are proportional to the raw total cross sections for full- and empty-target respectively. The latter two histograms were separately corrected, subtracted from one another and their difference used to measure the total cross section.

The main corrections are listed below:

(a) Some events resulted in interactions which prevented them from entering the above histograms. They are of three types. The first includes those that could not be identified because of microprocessor limitations and ambiguous chamber response. As mentioned above, these events were studied separately (off-line) and their number apportioned among interacting and non-interacting events. This apportioning yields a global correction, independent of the fine momentum structure at each setting. The second category includes the events which interact but were not entered in histogram M_1 because their scattering angle was smaller than the cut. The contribution to the cross section of these forward elastic events was evaluated on the basis of known total cross sections and elastic slopes from earlier experiments. The third category is that of inelastic events with one forward track; these were either included or excluded from the M_1 histogram depending on their scattering angle. The handle for the correction was provided by the veto box (VB) signal. Angular distributions were recorded with and without the VB signal(*). These were then used to evaluate the contribution of the above events to the total cross section.

(b) Beam muons and muons from $\pi \to \mu\nu$ decays after the target were identified by the counters behind the iron screen. However, a fraction of the pions were also responsible for S_μ signals via their hadronic cascade in the iron. This "punch-through" contribution was corrected on the basis of known rates observed in other experiments. The correction factor was of the order of a few tenths of one per cent at each momentum.

(*) Notice that δ rays generated in the target and emitted into the veto box give rise to spurious "inelastic" events. This effect is clearly visible in the angular distribution of the VB-on events as a sharp spike in the very forward direction $|t| \simeq 40$ MeV^2. These events were properly taken into consideration when accounting for the forward inelastic correction.

(c) The incident beam contained, in addition to the above muons, a small fraction of electrons, kaons and antiprotons. We have measured, with a series of Cerenkov counters, the relative abundance of these particles. Kaons and antiprotons were always less than $\sim$ 1%. Electrons, instead, were negligible above 5 GeV/c increasing rapidly below 5 GeV/c up to a maximum of $\sim$ 30% of the beam at 2 GeV/c. A functional momentum dependence was established for the electron content of the beam and a corresponding correction factor applied for each momentum bin.

(d) In addition to the above, other effects exist but with negligible consequences. The effect of δ rays emitted from the target towards the secondary chambers was seen to be practically eliminated by rejecting straight-through secondary tracks whether accompanied or not by other signals. The absorption in the target and associated material was cancelled by the empty-target subtraction.

The final total cross section is shown in fig. 3 as a function of momentum in bins of $dP/P = 5\ 10^{-4}$. The insets show in detail the typical full- and empty-target measurements (after correction) at two momentum settings. The overall normalization uncertainty ranges from 5 to 10%. Discontinuities in the momentum dependence can be noticed. They are particularly noticeable between sets of data taken far apart in time and under different beam conditions. No common and easily accountable cause could be traced to explain such discontinuities. The most likely conjecture is that the overall normalization at a given setting depends to a certain extent on the instantaneous beam intensity because of its effects on the chambers inefficiency. Notice that the measured inefficiency of each secondary chamber plane in the region close to the beam axis was of the order of 10^{-3}. The analysis demands at least two planes in order to reach a decision on the event. Thus, assuming the inefficiency of planes belonging to different chambers to be uncorrelated, the systematic uncertainty on the total cross section should be well below the statistical accuracy of $\pm$ 0.3 10^{-3}. However, a slow and systematic drift of this inefficiency over a long period of time may well go undetected and could account for the observed shift of the normalization. This being said, it should be stressed that the above discontinuities do not affect the experiment's aim which was a search for structures within <u>each</u> momentum setting.

In order to reach a quantitative estimate on the existence of narrow structures, we have performed a fit to the data of each setting. A linear momentum dependence was found to describe adequately the data. The distribution of the measurements around the expected values from the fit is shown in fig. 4(a) for all momenta together. A gaussian function has been fitted to this distribution and is shown superposed in the figure. The latter curve describes quite well the data, thus confirming that no narrow structures were present within the statistical significance of the measurements.

The sensitivity to resonances reached by the experiment is a function of the incident π^- momentum P and of the spin J and isospin I of the hypothetical resonance. Taking 6 standard deviations as a safe level of detection in view of our ~ 4500 data points, we arrive to the following relation for the minimum observable width Γ and elasticity $x = \Gamma_{el}/\Gamma$ of the resonance: $x\sqrt{\Gamma}\,(J + 1/2)/(I + 1/2) = A$, where A is an increasing function of P. If we express Γ in MeV and x in per cent, the value of A extends from ~ 7 at 2 GeV/c to ~ 100 at 14 GeV/c. As an example, fig. 4(b) shows the limiting values of Γ and x at 10 GeV/c (A = 60) for an I = 1/2 resonance of spin J = 1/2 to J = 11/2.

In conclusion, no significant structures have been observed in the π^-p total cross section between 2 and 14 GeV/c. The existence of nucleon resonances with large values of the spin can be excluded down to a few MeV in width and a few per cent in elasticity.

Acknowledgements

The support and advice of P. Fleury has been greatly appreciated.

REFERENCES

[1] P. Baillon et al., CERN/EP/80- (in preparation), to be submitted to Phys. Lett. B.

FIGURE CAPTIONS

Fig. 1 Side view of the apparatus. The set-up shown in fig. 1 of ref. [1], though not drawn, is in place. Only the last portion of the focusing spectrometer is shown here, together with the specific equipment used for the total cross section measurement. The first beam chamber (W_1), not shown, is $\sim$ 24 m upstream of the target. A vacuum pipe joins the W_2 and W_3 chambers, helium bags are inserted between W_3 and the target and between the exit of the veto box (VB) and the downstream chamber WF_2. The ST_3 counter was used for monitoring and testing purposes. The other elements are described in the text.

Fig. 2 Some of the histograms generated by the on-line microprocessor analysis at 4.11 GeV/c, with full- and empty-target. The meaning of the histograms is described in the text.

Fig. 3 Corrected and normalized $\pi^- p$ total cross section versus incident π^- laboratory momentum. The momentum scale is logarithmic, so as to yield an equal spacing between measurements. The spacing corresponds to fractional momentum bins of $5 \cdot 10^{-3}$. The systematic normalization uncertainty ranges from 5 to 10%. The insets show an expanded view of the raw data at selected momenta. Results from other experiments are shown with dotted error bars.

Fig. 4 (a) Residuals ξ of the fit described in the text. Resonances should manifest themselves as large positive values of ξ.

(b) Elasticity x as a function of width Γ for I = 1/2 nucleon resonances of spin J at the limit of our detection sensitivity (6 standard deviations).

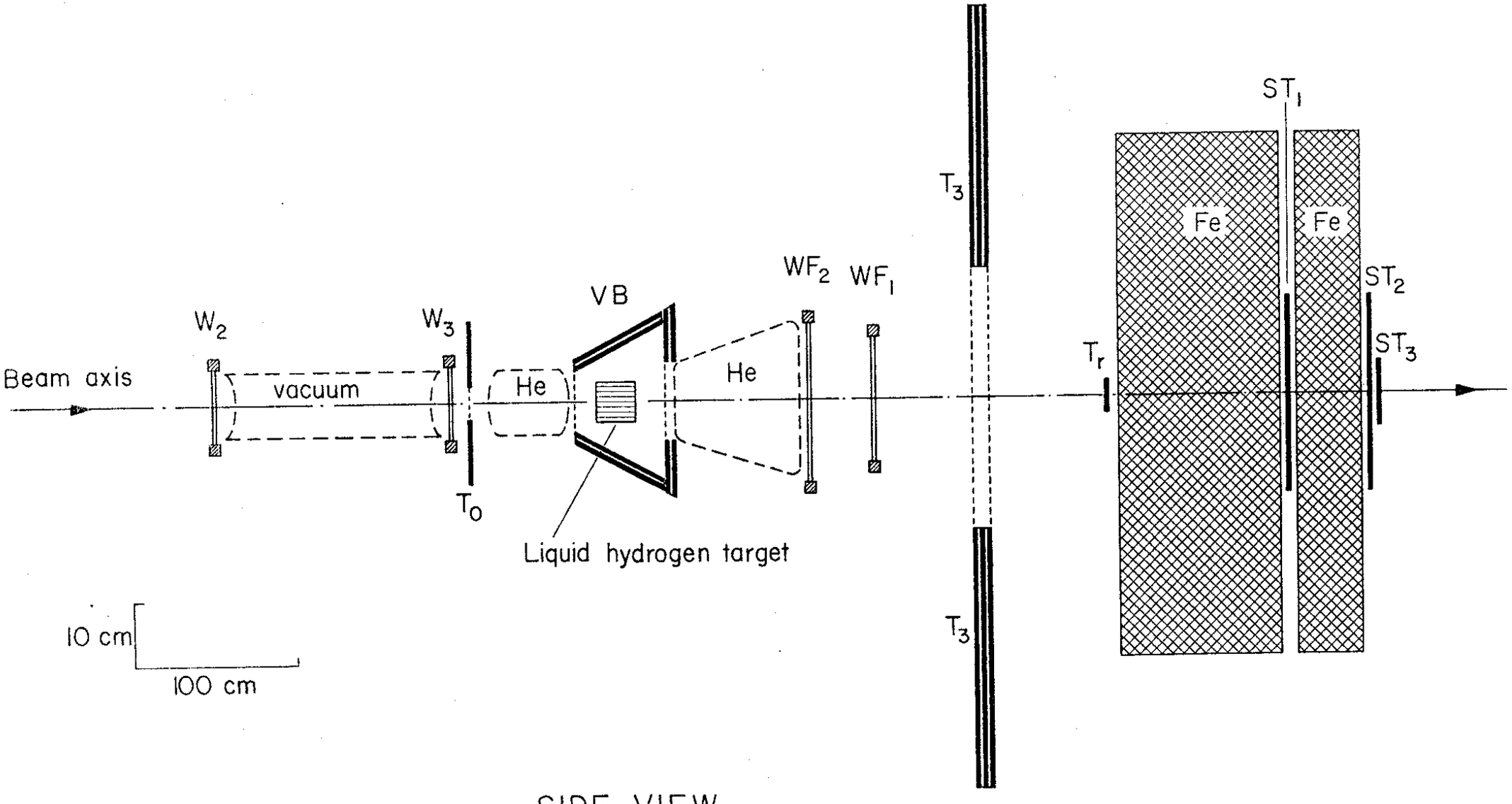

SIDE VIEW

Fig. 1

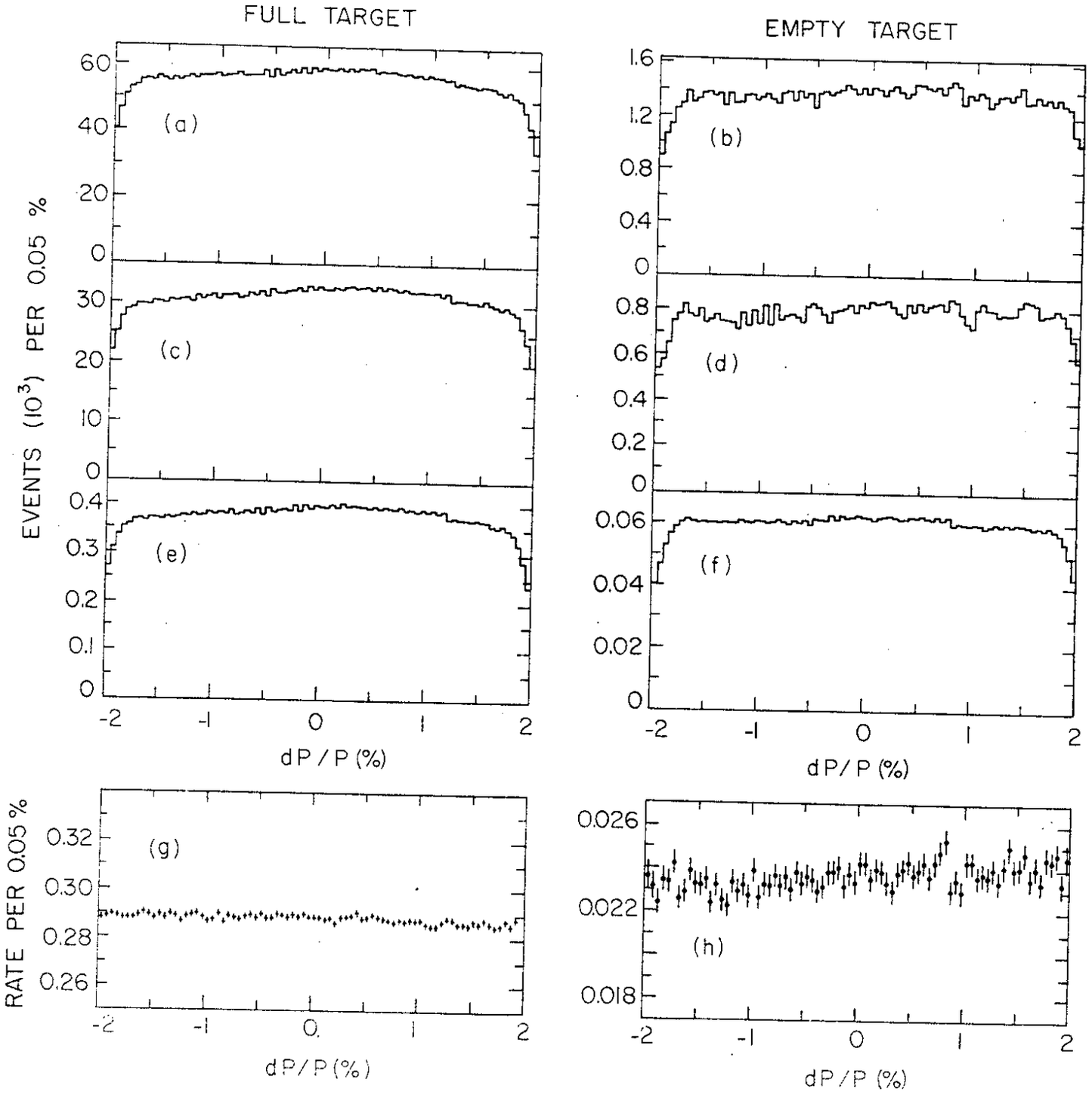
FULL TARGET
EMPTY TARGET
EVENTS (10³) PER 0.05 %
RATE PER 0.05 %
(a)
(b)
(c)
(d)
(e)
(f)
(g)
(h)
dP / P (%)
dP/P (%)

Fig. 2

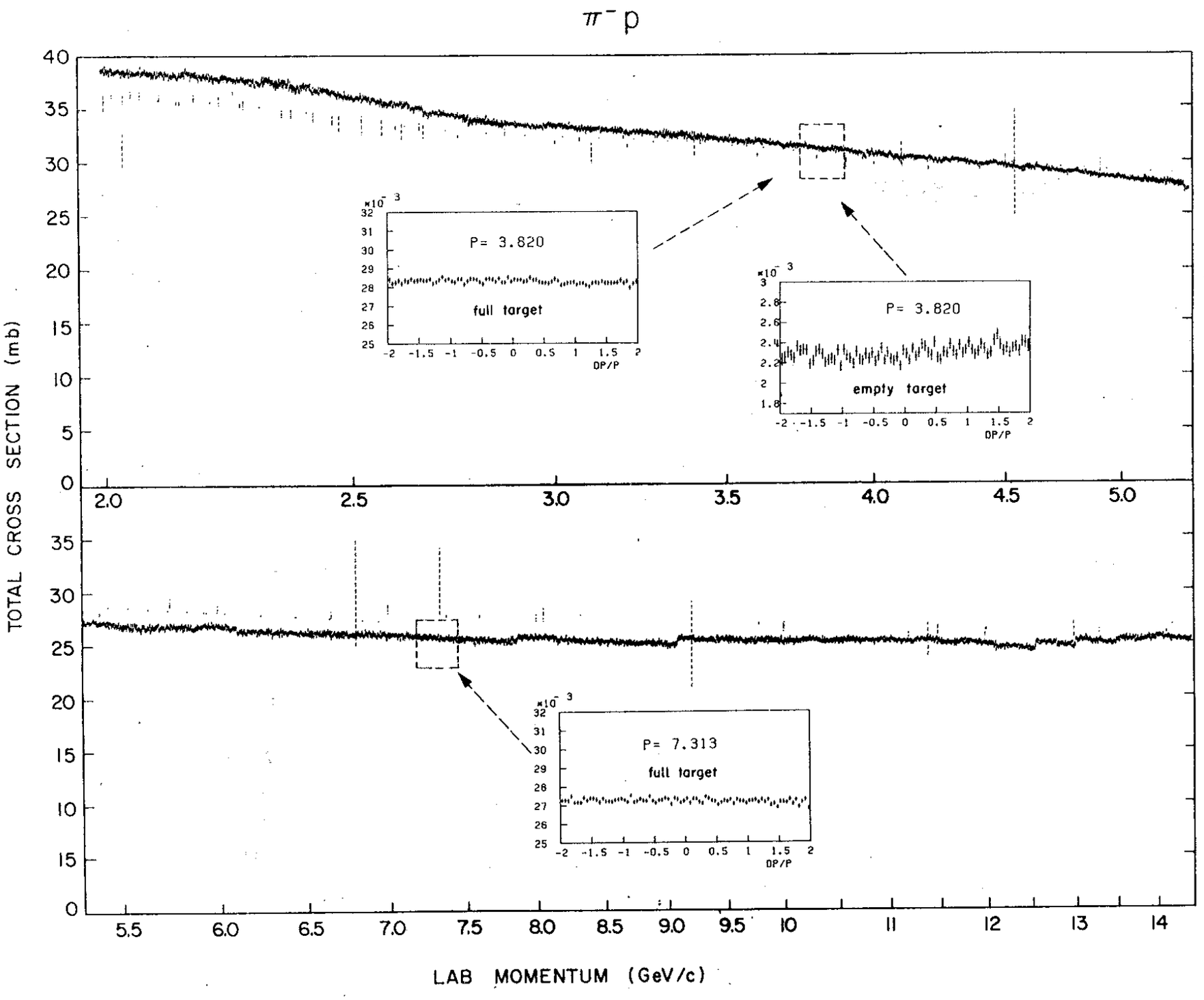
$\pi^- p$
TOTAL CROSS SECTION (mb)
LAB MOMENTUM (GeV/c)
P= 3.820
full target
P= 3.820
empty target
P= 7.313
full target
DP/P

Fig. 3

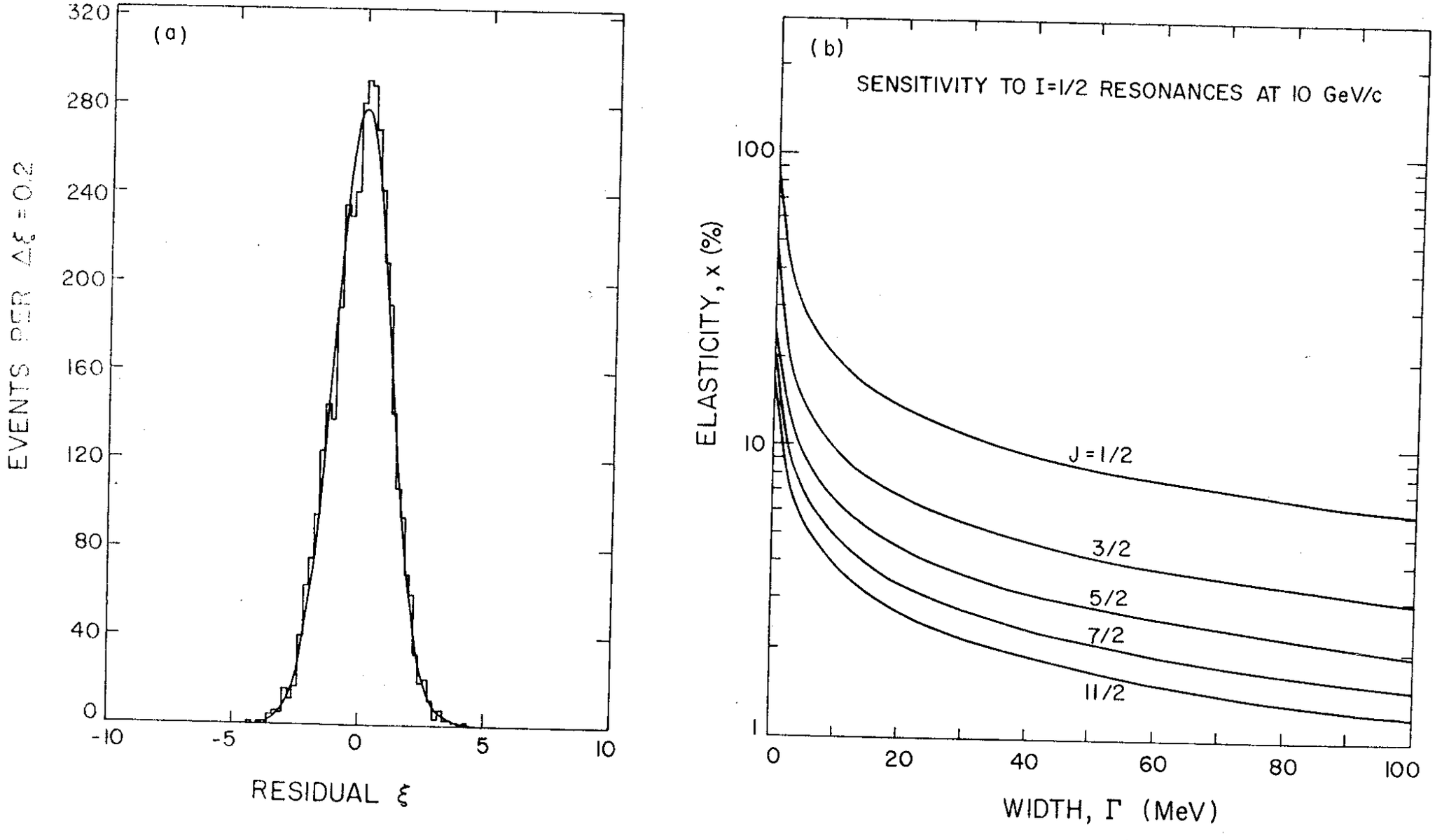
(a)
EVENTS PER Δξ = 0.2
320
280
240
200
160
120
80
40
0
-10
-5
0
5
10
RESIDUAL ξ
(b)
SENSITIVITY TO I=1/2 RESONANCES AT 10 GeV/c
ELASTICITY, x (%)
100
10
1
J = 1/2
3/2
5/2
7/2
11/2
0
20
40
60
80
100
WIDTH, Γ (MeV)

Fig. 4